Irregular topography at the Earth's inner core boundary

Zhiyang Dai[a,b,1], Wei Wang[a,1], and Lianxing Wen[a,b,2]

[a]School of Earth and Space Sciences, University of Science and Technology of China, Hefei, Anhui 230026, China; and [b]Department of Geosciences, State University of New York at Stony Brook, Stony Brook, NY 11794

Edited by Don Helmberger, California Institute of Technology, Pasadena, CA, and approved March 27, 2012 (received for review October 4, 2011)

Compressional seismic wave reflected off the Earth's inner core boundary (ICB) from earthquakes occurring in the Banda Sea and recorded at the Hi-net stations in Japan exhibits significant variations in travel time (from −2 to 2.5 s) and amplitude (with a factor of more than 4) across the seismic array. Such variations indicate that Earth's ICB is irregular, with a combination of at least two scales of topography: a height variation of 14 km changing within a lateral distance of no more than 6 km, and a height variation of 4–8 km with a lateral length scale of 2–4 km. The characteristics of the ICB topography indicate that small-scale variations of temperature and/or core composition exist near the ICB, and/or the ICB topographic surface is being deformed by small-scale forces out of its thermocompositional equilibrium position and is metastable.

inner core growth | geodynamo | outer core convection

The Earth's inner core grows from the solidification of the liquid outer core (1). The solidification process releases latent heat and expels light elements, providing driving forces for the thermocompositional convection in the outer core (2, 3) and the geodynamo that is responsible for the Earth's magnetic field (4–6). Information about the inner core boundary (ICB) is thus the key to the understanding of driving forces in outer core convection. The ICB has always been thought to be flat, simple, and smooth, due to the presumed extremely small variation in temperature in the outer core (7). Although recent seismic observations provide indirect evidence for the existence of topography at the ICB based on the localized temporal changes of the inner core surface (8–10), direct seismic observations about the existence of inner core topography are still nonexistent. Here, we used PKiKP (a seismic compressional wave reflected from the ICB, Fig. 1*A*) recorded in precritical distances to study inner core topography.

Results

In the precritical distances, PKiKP travel times and amplitudes are sensitive to topography, geometry, and property contrast across the ICB (11–16). We adopted PcP waves [a compressional wave that is reflected off the core-mantle boundary (CMB)] as a reference phase and used PKiKP-PcP differential travel time and relative amplitude to study the ICB property. The use of differential PKiKP-PcP travel time and relative PKiKP/PcP amplitude ratio minimizes the effects of shallow Earth's structure and uncertainties in source origin time, location, magnitude, and radiation pattern (refs. 17–22; Fig. 1*A*).

We collected all available PKiKP-PcP data from earthquakes occurring in the Banda Sea and recorded at the Hi-net stations in Japan during 2004–2010. The selected earthquakes have a depth range from 100 to 650 km, with magnitudes ranging between 5.8 and 7.6 (Table 1). We measured PKiKP-PcP differential times on the vertical components of seismic data. The seismic data were filtered with a two-pole causal Butterworth band-pass filter of 1–3 Hz and the worldwide standard seismic network short-period instrument response. These filtering procedures were adopted after extensive testing of various filters for the best observability of the PKiKP phases. We visually checked PKiKP and PcP phases for quality; only those with high signal-to-noise ratios were retained for further analyses. To ensure the reliability of phase selection, we adopted the following procedures in travel time selection. We first handpicked the seismic phases and stacked seismic waveforms along the handpicked seismic phases; we then reselected the seismic phase in each seismic observation based on its cross-correlation with the stacked seismic waveform. The stacking and reselection procedures were repeated until excellent cross-correlation values were obtained and travel time selections no longer changed. The seismic waveforms were aligned according to the cross-correlation selections and were further checked for possible cycle skipping. The data with any possibility of cycle skipping were discarded. Following these procedures, we retained a total of 128 high-quality PKiKP-PcP waveforms pairs from three earthquakes: January 27, 2006, August 4, 2008, and August 28, 2009 (Fig. 1*B*). The selected PKiKP waves sample a 7° by 10° region at the ICB between 12–19°N and 126–136°E (Fig. 1*B*). The selected data exhibit high-quality PKiKP and PcP waveforms and have excellent correlations with their stacked waveforms. One example of PKiKP and PcP seismogram profiles from event January 27, 2006 is shown in Fig. 1 *C* and *D*.

PKiKP-PcP differential time residuals exhibit large variations across the seismic array, varying from −2 to 2.5 s (Fig. 2*A*). The relative PKiKP/PcP amplitudes also vary considerably across the array, changing by at least a factor of 4 from 0.2 to 0.05, very different from the predictions based on Preliminary Reference Earth Model (PREM) (ref. 23; Fig. 2*B*). Both the differential travel times and amplitude ratios show a spatially complicated pattern, varying at a small length scale (less than 1°, Fig. 2 *A* and *B*).

The use of differential travel times and relative amplitudes of the PKiKP and PcP phases minimizes many uncertainties as we mentioned above; however, the differential signals could still be attributed to the seismic structures either at the CMB or at the ICB, or both. Several lines of evidence indicate that the observed PKiKP-PcP differential signals are mainly caused by the ICB structures, rather than the seismic structures in the mantle. (*i*) The PKiKP-PcP differential travel time residuals positively correlate with the PKiKP travel time residuals (Fig. 3 *A*, *C*, and *E*), whereas no correlation is observed with the PcP travel time residuals (Fig. 3 *B*, *D*, and *F*). In addition, the variations of PcP travel time residuals are on an order of about 1.5 s (Fig. 3 *B*, *D*, and *F*), much less than the magnitude of the observed PKiKP-PcP differential travel time residuals. These observations suggest that the PKiKP-PcP differential travel time residuals are most likely contributed by the PKiKP phases, rather than the PcP phases. (*ii*) We calculated the effects of mantle heterogeneities on the PKiKP-PcP differential times based on various global compres-

Author contributions: L.W. designed research; Z.D., W.W., and L.W. performed research; Z.D. and W.W. analyzed data; and Z.D., W.W., and L.W. wrote the paper.

The authors declare no conflict of interest.

This article is a PNAS Direct Submission.

[1]Z.D. and W.W. contributed equally to this work.

[2]To whom correspondence should be addressed. E-mail: Lianxing.Wen@sunysb.edu.

This article contains supporting information online at www.pnas.org/lookup/suppl/doi:10.1073/pnas.1116342109/-/DCSupplemental.

EARTH, ATMOSPHERIC, AND PLANETARY SCIENCES

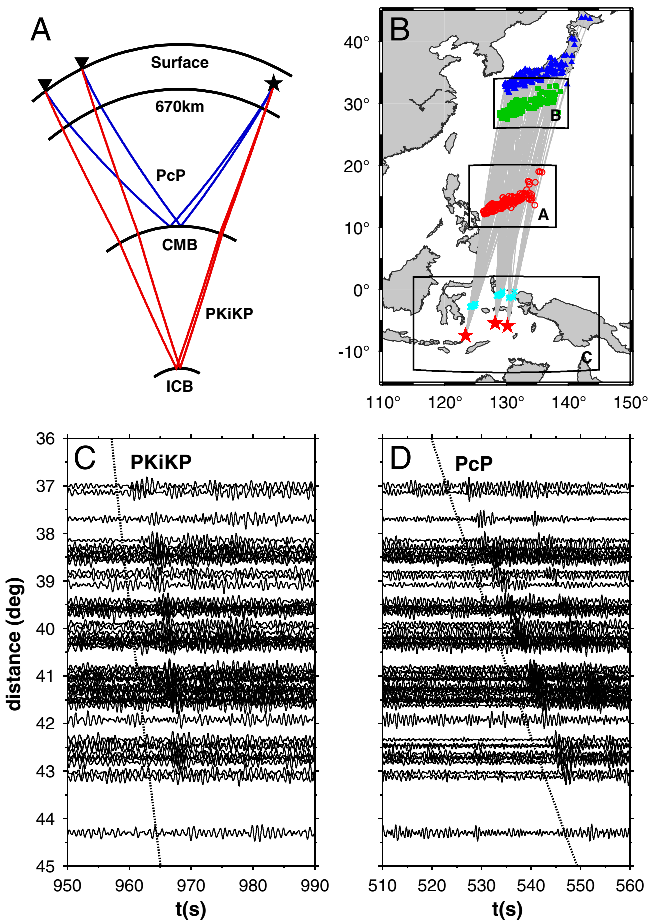

Fig. 1. (*A*) Ray paths of PKiKP (red) and PcP (blue) waves at epicentral distances of 40° and 48°. CMB and ICB represent the core-mantle boundary and the inner core boundary, respectively. (*B*) Map view of great-circle ray paths (gray lines) for the PKiKP waves from earthquakes occurring in the Banda Sea (red stars) to the Hi-net stations (blue triangles) in Japan. Red circles indicate the PKiKP bouncing points at the ICB, and light blue crosses and green squares represent PKiKP entrance and exit points across the CMB. Only those ray paths with both high-quality PcP and PKiKP waveforms are plotted. Boxes A, B, C correspond to the CMB regions studied in Fig. 4 *A*–*C*, respectively. (*C* and *D*) Waveforms of PKiKP (*C*) and PcP (*D*) waves observed for event January 27, 2006. The dashed lines indicate the theoretical PKiKP and PcP arrival times with respect to PREM (23). Waveforms are band-pass filtered from 1–3 Hz and with the worldwide standard seismic network short-period instrument response.

sional wave models. Mantle effects on the PKiKP-PcP differential travel times are on an order of 0.2 s. These variations are an order of magnitude smaller than the observed PKiKP-PcP differential travel time variations and the corrected PKiKP-PcP differential travel times change little from the observed values (see two examples after the corrections using two compressional models in Fig. S1). (*iii*) Further quantification of the effects of the CMB structures on the PcP travel times indicates that the CMB structures in the PcP reflected region indeed contribute little to the lateral variation of the PKiKP-PcP differential travel times. We analyzed the difference of PcP travel time residuals recorded at the same stations between the neighboring events in the Banda Sea. Because event separations were small (within 2°, Table 1), the difference of PcP travel time residuals recorded at a same station between two neighboring events reflect the lateral variations of the seismic structures between their respective CMB reflected points of the event pair and difference of seismic structures in their source lags (see an example of PcP ray paths for two neighboring events in the top left inset in Fig. 4*A*). The

Table 1. Event parameters

Event date	Time	Latitude. °N	Longitude, °E	Depth, km	Magnitude
03/02/05	10:42:12	−6.54	129.99	196	7.1
01/15/06	11:58:29	−7.88	122.58	262	6.2
01/27/06*	16:58:54	−5.45	128.19	404	7.6
07/15/06	07:10:48	−4.39	126.31	385	5.8
09/09/06	04:13:12	−7.23	120.27	583	6.3
11/14/06	14:21:02	−6.34	127.99	353	6.1
07/01/07	14:34:12	−5.97	130.55	142	5.9
12/15/07	08:03:17	−7.78	127.54	190	6.0
04/29/08	19:10:03	−6.22	127.56	428	5.8
06/06/08	13:42:48	−7.49	127.89	122	6.0
08/04/08*	20:45:13	−5.92	130.20	174	6.1
12/06/08	10:55:26	−7.39	124.75	398	6.4
07/06/09	22:35:04	24.87	128.03	7	6.0
08/28/09*	01:51:20	−7.15	123.43	642	6.9
10/24/09	14:40:43	−6.13	130.39	130	6.9
02/15/10	21:51:47	−7.22	128.72	126	6.2
02/26/10	20:31:26	25.93	128.43	25	7.0
05/26/10	08:53:08	25.77	129.94	10	6.2
06/27/11†	16:47:14	−8.93	122.47	120	5.8

*Earthquakes used for PKiKP-PcP analysis.
†Earthquake used for PKP precursory energy analysis.

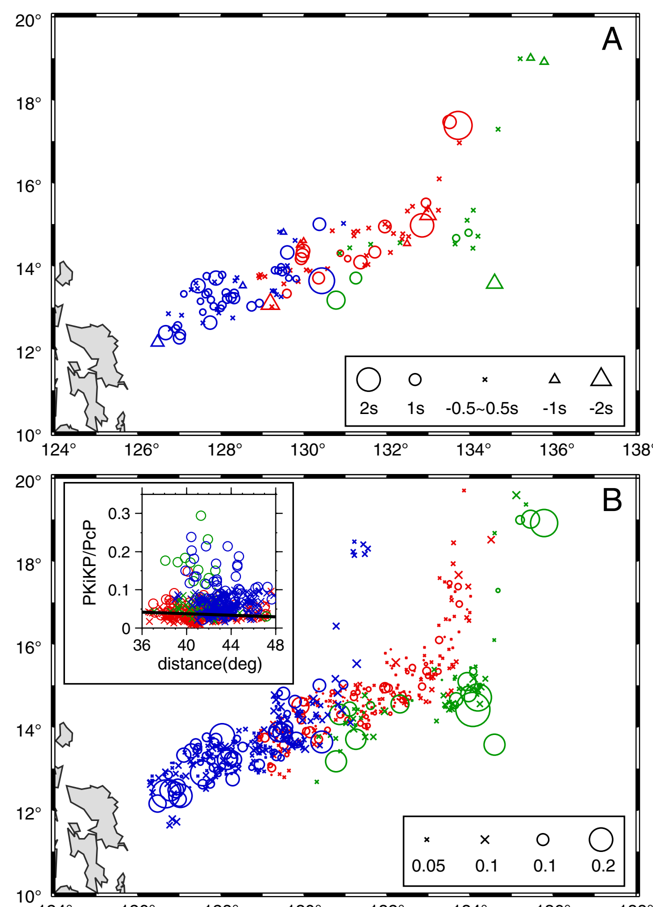

Fig. 2. (*A*) PKiKP-PcP differential travel time residuals with respect to PREM, plotted at the PKiKP bouncing points of the ICB. (*B*) PKiKP/PcP amplitude ratios, plotted at PKiKP bouncing points of the ICB; circles denote the amplitude ratios of the reliably observed PKiKP and PcP phases; plus symbols show the amplitude ratios of invisible PKiKP and clear PcP, which should be considered as a lower bound of the amplitude ratio. The data are color-coded as earthquakes: January 27, 2006 (red), August 4, 2008 (green), and August 28, 2009 (blue). The amplitude ratios are also plotted in the inset as a function of epicentral distance, along with the predictions based on PREM (thick line).

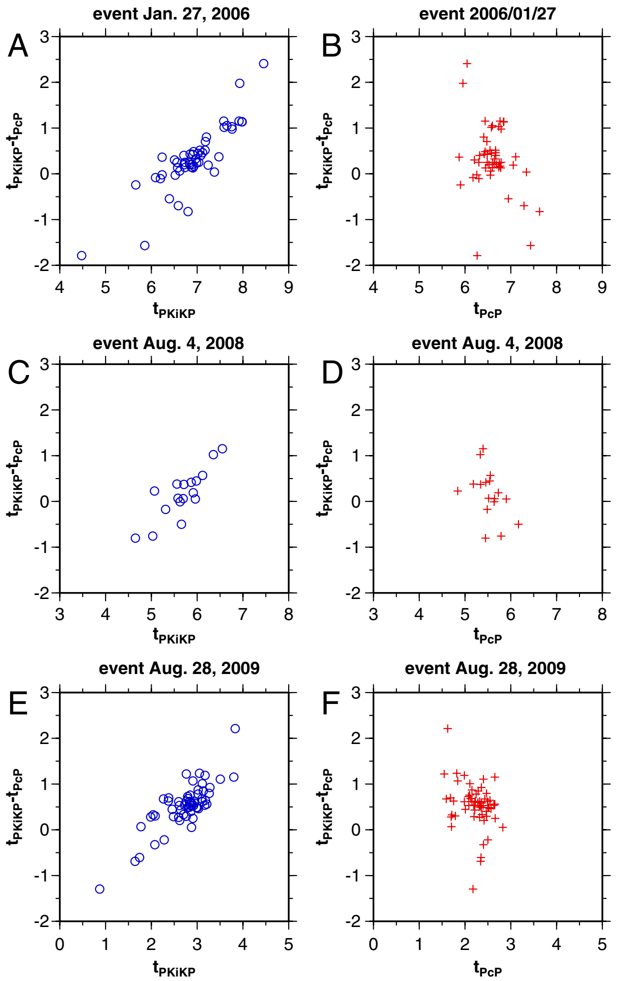

Fig. 3. Relationship between PKiKP-PcP differential travel time residuals and PKiKP travel time residuals (both with respect to PREM) for events January 27, 2006 (*A*), August 4, 2008 (*C*), and August 28, 2009 (*E*). (*B*, *D*, and *F*) Same as *A*, *C*, and *E*, except for the relationship between differential PKiKP-PcP travel time residuals and PcP travel time residuals.

differences of PcP travel time residuals for four event pairs in the Banda Sea exhibit little difference in their PcP travel time residuals, ranging from −0.2 to 0.2 s (Fig. 4*A*). These variations are an order of magnitude smaller than those observed in the PKiKP-PcP differential travel time residuals, indicating that the observed PKiKP-PcP differential travel time residuals are contributed little by the seismic structures in the PcP reflected area of the CMB. (*iv*) We studied the effects of the seismic heterogeneities in the CMB region near the PKiKP exit points on the PKiKP travel time residuals by analyzing the travel time residuals of the PcP phases sampling the same region. We were able to find several events whose PcP reflected points partially overlay with the PKiKP exit points (Fig. 4*B*). Note that a variation of −0.4 to 0.4 s is observed in the PcP travel time residuals (with respect to PREM) across the array (Fig. 4*B*), similar to what is observed for the PcP phases recorded for the Banda Sea events. As the PcP phases sample the CMB region twice, the observed magnitude of the PcP travel time variations sampling the same region indicate that the contributions from the receiver-side CMB region is also at least an order of magnitude smaller than the observed PKiKP-PcP differential travel time residuals. (*v*) We studied the effects of small-scale seismic heterogeneities in the CMB region near the PKiKP entrance points by analyzing the PKP (a compressional wave traveling inside the Earth's inner core) precursory energy from a seismic event in the region recorded in the United States

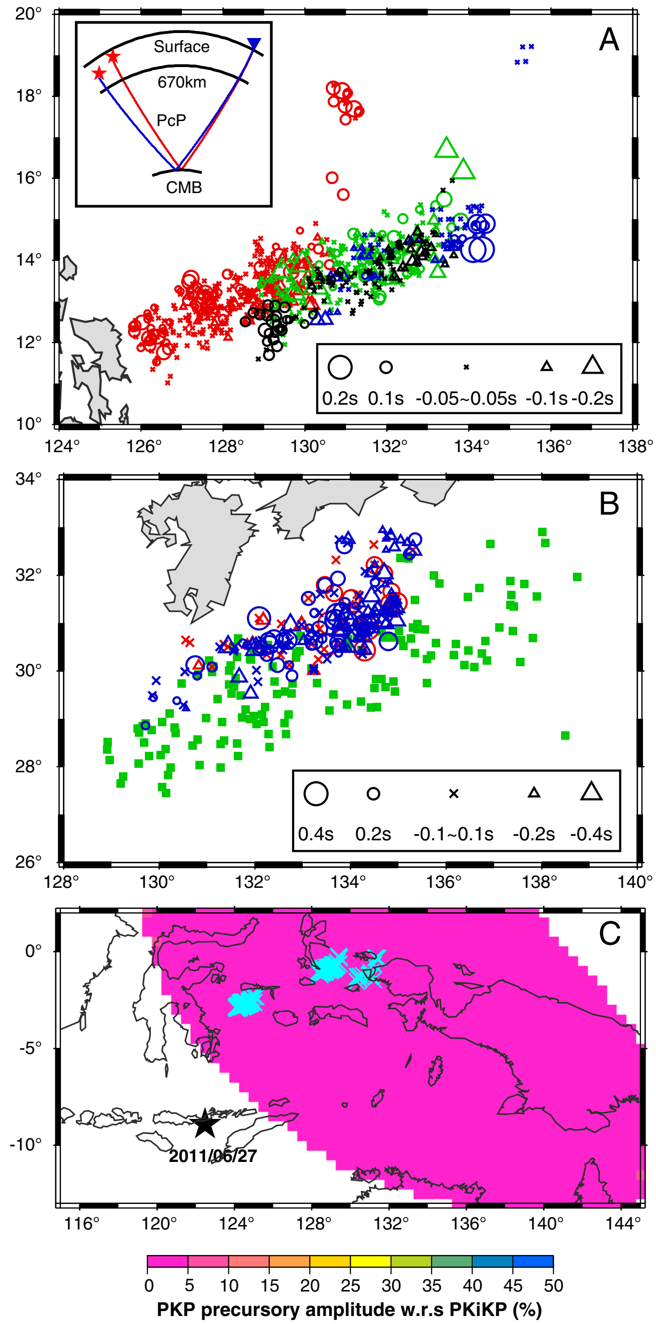

Fig. 4. Analyses of small-scale seismic heterogeneities in the CMB regions near the PcP reflected points (*A*), PKiKP exit points (*B*), and PKiKP entrance points (*C*) for the seismic phases from the Banda Sea events to the Hi-net stations. *A*, *B*, and *C* correspond to the boxed regions labeled as A, B, C in Fig. 1*B*. (*A*) Difference between PcP travel time residuals (with respect to PREM) between neighboring events, plotted at the PcP reflected points of the CMB. Red symbols are for event pair of January 15, 2006 and August 28, 2009, green symbols for event pair January 27, 2006 and February 15, 2010, blue symbols for event pair July 1, 2007 and August 4, 2008, and black symbols for event pair December 15, 2007 and June 6, 2008. The top left inset shows PcP ray paths for an event pair whose distance separation is 2°. (*B*) Variations of PcP travel time residual with respect to PREM, plotted at the PcP reflected points at the CMB. Symbols are color-coded with different events (Table 1). Green squares represent PKiKP exit points at the CMB from the Banda Sea events. (*C*) PKP precursory amplitudes with respect (w.r.s.) to the main PKP phases (the ratio between the two amplitudes) obtained from migration of the observations recorded in 12 high-quality stations in the United States (Table S1) from an event in the region (star labeled June 27, 2011 and Table 1). The light-blue crosses represent the PKiKP entrance points at the CMB of the three events in the Banda Sea to the Hi-Net stations.

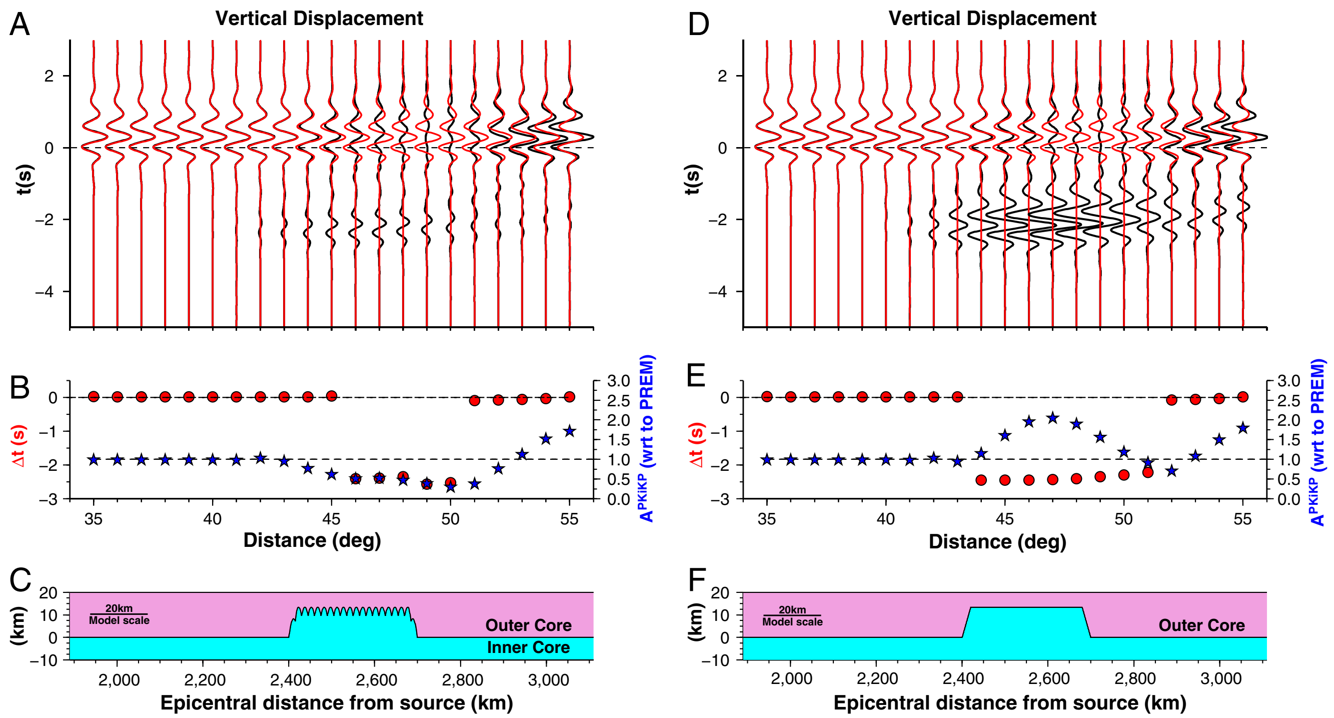

Fig. 5. (*A*) Synthetic vertical component of PKiKP seismograms at the distance range from 35° to 55° for PREM (red traces) and a model with ICB topography shown in *C* (black traces). The black traces are normalized with respect to (wrt) the amplitudes of PKiKP synthetics based on PREM. Traces are band-passed filtered with the same filtering procedures applied to the data and aligned along the predicted PKiKP arrival times based on PREM ($t = 0$). (*B*) PKiKP travel time residuals (red dots, left scale) and amplitudes (blue stars, right scale) with respect to the PREM predictions at various epicentral distances. (*C*) ICB topographic model plotted as a function of distances from the seismic source, which also correspond to the PKiKP reflected points for the distances of the synthetics at *A* and *B*. (*D*–*F*) Same as *A*–*C*, except that the ICB topographic model has a superimposed small-scale topography with a height variation of 4 km repeated with a horizontal length scale of 3 km. Note the amplitude differences in the distance range of 43° to 52° between the synthetics in *A* and *D*.

(Fig. 4*C*). The PKP data are band-passed filtered with the same frequencies used for analyzing the PKiKP data recorded in the Hi-net stations to probe possible existence of small-scale seismic structures in the same wavelengths. The energy proceeding the PKP phases was mapped onto the CMB regions based on a migration method (24). The amplitude preceding the PKP phases exhibited less than 5% of the amplitude of the main phases, similar to that of the background noise. The lack of proceeding energy before the PKP phases indicates that the CMB region exhibits little small-scale variations of seismic structure (Fig. 4*C*) and the PKiKP-PcP differential travel times observed in the Hi-net stations were not caused by the seismic structures in the PKiKP entrance points of the CMB region. With all these possible mantle effects examined, we concluded that the observed PKiKP-PcP differential travel time residuals and amplitude ratios from the Banda Sea events to the Hi-net stations were mostly caused by the seismic structures at the ICB.

The observed PKiKP travel time variations indicate that the ICB possesses topography in the PKiKP reflected region. The observed PKiKP amplitude variations and rapid changes of PKiKP travel time and amplitude across the seismic array further indicate that the ICB topography is irregular and varies at a small length scale. We tested a series of ICB models to place quantitative bounds on the characteristics of the ICB topography, using a hybrid method (*Materials and Methods*) (25). We tested ICB topographic models with various geometries (Gaussian-shaped, dome-shaped, step), heights, horizontal scales, and spatially repeated patterns. A change of topographic height of 14 km is required to explain the observed 2.5-s variation of PKiKP travel time (Fig. 5). A change of topographic height in a horizontal distance of no more than 6 km is required to explain the rapid spatial variation of PKiKP travel time in the observations. The magnitude of the PKiKP amplitude change and its frequency content require a superposition of small-scale topography with a height variation of 4–8 km and a horizontal spacing of about 2–4 km to reduce the PKiKP amplitude by a factor of 4 (Fig. 5).

Discussion

PKiKP phase has been enigmatic in its observability in the precritical distances (16–22, 26–29). Although its observability was predicted based on the elastic parameters of Earth's models, it was only occasionally observed when the seismic station coverage was sparse, which can be explained by the characteristics of the ICB topography inferred here. A mosaic structure of the inner core's surface was also invoked to explain the strong PKiKP amplitude variations observed in the precritical distance ranges (16). Our results indicate that the existence of small-scale topography at the ICB, as required by the observed PKiKP travel time variations in the precritical distances, could also provide an explanation to the observed strong variability of the PKiKP amplitudes in the precritical distances without invoking a mosaic ICB structure. The magnitude of the ICB topography was inferred to be at least in an order of from 0.98–3 km based on the magnitude of the observed temporal change (8, 9), and the horizontal length-scale of the ICB topography was estimated to be about 10 km based on the Fresnel zone associated with the seismic frequencies of the ICB reflections (9). Our results not only provide direct seismic evidence confirming those inferences, but also reveal a more complete picture about the irregularities of the ICB. However, this study region occupies only a small patch of the ICB surface; a global survey of the characteristics of the inner core surface is needed.

The existence of irregular topography at the ICB indicates two possible scenarios of dynamic and thermochemical conditions near the ICB. (*i*) The ICB represents a phase boundary in equilibrium with local temperature and core compositions. In this scenario, the existence of ICB topography would require existence of small-scale variations of temperature and/or core composition near the ICB. (*ii*) Small-scale dynamic forces deform the phase boundary that is in equilibrium with temperature and core compositions out of the equilibrium position and form the irregular topography, and the timescales of dynamic deformation are smaller than what is required for the deformed boundary to adjust to thermochemical equilibrium with local temperature and core compositions (i.e., melting or solidifying). In this scenario, the ICB topographic surface is metastable.

Materials and Methods

We use the hybrid method developed by Wen and Helmberger (25) to calculate synthetic seismograms. The hybrid method is a combination of analytic methods (the generalized ray theory and the Kirchhoff method) and a finite-difference (FD) method, with the FD calculations applied to the heterogeneous media in the deep mantle. In this case, the FD region encompasses portions of the bottom of the outer core and the top of the inner core. The Kirchhoff theory is applied to the upper FD region to bring the wavefields back to the surface.

Seismic data are obtained from the Hi-net stations (http://www.hinet.bosai.go.jp/). Seismic data are deconvolved with their respective instrumental responses.

ACKNOWLEDGMENTS. We thank the editor and two anonymous reviewers for their comments, which have significantly improved the paper, and the Japanese Hi-net for providing the seismic data. This work was supported by the National Natural Science Foundation of China under Grants NSFC41130311 and NSFC40904008 and the Chinese Academy of Sciences and State Administration of Foreign Experts Affairs International Partnership Program for Creative Research Teams.

1. Jacobs JA (1953) The Earth's inner core. *Nature* 172:297–298.
2. Braginsky SI (1963) Structure of the F layer and reasons for convection in the Earth's core. *Dokl Akad Nauk SSSR* 149:8–10.
3. McFadden PL, Merrill RT (1986) Geodynamo source constraints from paleomagnetic data. *Phys Earth Planet Inter* 43:22–33.
4. Gubbins D (1977) Energetics of Earth's core. *J Geophys* 43:453–464.
5. Loper DE (1978) Gravitationally powered dynamo. *Geophys J R Astron Soc* 54:389–404.
6. Moffatt HK, Loper DE (1994) The magnetostrophic rise of a buoyant parcel in the Earth's core. *Geophys J Int* 117:394–402.
7. Stevenson DJ (1987) Limits on lateral density and velocity variations in the Earth's outer core. *Geophys J R Astron Soc* 88:311–319.
8. Wen L (2006) Localized temporal change of the earth's inner core boundary. *Science* 314:967–970.
9. Cao AM, Masson Y, Romanowicz B (2007) Short wavelength topography on the inner-core boundary. *Proc Natl Acad Sci USA* 104:31–35.
10. Song XD, Dai W (2008) Topography of Earth's inner core boundary from high-quality waveform doublets. *Geophys J Int* 175:386–399.
11. Engdahl ER, Flinn EA, Romney CF (1970) Seismic waves reflected from Earth's inner core. *Nature* 228:852–1053.
12. Cummins P, Johnson LR (1988) Short-period body wave constraints on properties of the Earth's inner core boundary. *J Geophys Res* 93:9058–9074.
13. Cummins P, Johnson L (1988) Synthetic seismograms for an inner core transition of finite thickness. *Geophys J* 94:21–34.
14. Souriau A, Souriau M (1989) Ellipticity and density at the inner core boundary from subcritical PKiKP and PcP data. *Geophys J Int* 98:39–54.
15. Shearer P, Masters G (1990) The density and shear velocity contrast at the inner core boundary. *Geophys J Int* 102:491–498.
16. Krasnoshchekov DN, Kaazik PB, Ovtchinnikov VM (2005) Seismological evidence for mosaic structure of the surface of the Earth's inner core. *Nature* 435:483–487.
17. Engdahl ER, Flinn EA, Masse RP (1974) Differential PKiKP travel times and radius of inner core. *Geophys J R Astron Soc* 39:457–463.
18. Koper KD, Pyle ML, Franks JM (2003) Constraints on aspherical core structure from PKiKP-PcP differential travel times. *J Geophys Res* 108:2168.
19. Koper KD, Franks JM, Dombrovskaya M (2004) Evidence for small-scale heterogeneity in Earth's inner core from a global study of PKiKP coda waves. *Earth Planet Sci Lett* 228:227–241.
20. Koper KD, Pyle ML (2004) Observations of PKiKP/PcP amplitude ratios and implications for Earth structure at the boundaries of the liquid core. *J Geophys Res* 109:B03301.
21. Koper KD, Dombrovskaya M (2005) Seismic properties of the inner core boundary from PKiKP/P amplitude ratios. *Earth Planet Sci Lett* 237:680–694.
22. Kawakatsu H (2006) Sharp and seismically transparent inner core boundary region revealed by an entire network observation of near-vertical PKiKP. *Earth Planets Space* 58:855–863.
23. Dziewonski AM, Anderson DL (1981) Preliminary reference Earth model. *Phys Earth Planet Inter* 25:297–356.
24. Wen L (2000) Intense seismic scattering near the Earth's core-mantle boundary beneath the Comoros hotspot. *Geophys Res Lett* 27:3627–3630.
25. Wen L, Helmberger DV (1998) A two-dimensional P-SV hybrid method and its application to modeling localized structures near the core-mantle boundary. *J Geophys Res* 103:17901–17918.
26. Buchbinder GGR, Wright C, Poupinet G (1973) Observations of PKiKP at distances less than 110°. *Bull Seismol Soc Am* 63:1699–1707.
27. Choy GL, Cormier VF (1983) The structure of the inner core inferred from short-period and broad-band GDSN data. *Geophys J R Astron Soc* 72:1–21.
28. Poupinet G, Kennett BLN (2004) On the observation of high frequency PKiKP and its coda in Australia. *Phys Earth Planet Inter* 146:497–511.
29. Tkalcic H, Kennett BLN, Cormier VF (2009) On the inner-outer core density contrast from PKiKP/PcP amplitude ratios and uncertainties caused by seismic noise. *Geophys J Int* 179:425–443.